Discerning the internal spatial heavy-atom effect on the organic phosphorescence of 9-phenylcarbazole by transient absorption spectroscopy

Yang Liu, Zhinan Jiang, Lina Ding, Yonggang Yang,* Tiantian Guan, Chaochao Qin,† and Yufang Liu‡

Henan Key Laboratory of Infrared Materials & Spectrum Measures and Applications, School of Physics, School of Chemistry and Chemical Engineering, Henan Normal University, Xinxiang 453007, People's Republic of China

(Received 28 September 2023; revised 23 February 2024; accepted 27 February 2024; published 19 March 2024)

Enhancing spin-orbital coupling by heteroatom and heavy-atom effects plays a critical role in organic room-temperature phosphorescence. Herein, a nitrogen-hybridized 9-phenylcarbazole (**1**), and its bromine-substituted derivatives on the 9-phenyl moiety (*ortho*-**4**, *meta*-**3**, *para*-**2**) and carbazole moiety (**5**, **6**, **7**), are studied by transient absorption (TA) spectroscopy. For 9-phenylcarbazole, the presence of excited-state-absorption (610 nm) and triplet-triplet-absorption (400 nm) signals in TA spectroscopy indicates the occurrence of intersystem crossing (ISC) with a lifetime of about 10 ns. After Br substitution in the 9-phenyl moiety, the ISC lifetime follows the order of compound **2** (4.9 ns) > compound **3** (1.9 ns) > compound **4** (0.74 ns), implying that the heavy-atom effect enhances with decreasing distance between the Br atom and core carbazole moiety. For carbazole-substituted derivatives, the ISC lifetimes of compounds **5** and **6** significantly decrease to 0.05171 and 0.01185 ns, respectively, demonstrating that the bromine substituent in the carbazole core results in a more efficient heavy-atom effect. However, the lifetime of the triplet exciton decreases with the enhancement of ISC efficiency. Compared to compound **5**, the ISC lifetime of biphenyl-structured compound **7** (53.35 ps) shows a slight change, whereas the triplet-exciton lifetime of compound **7** (183.3 ns) increases by approximately 40 times. The decrease in the Hung-Rhys factor and reorganization energies confirms that the biphenyl structure hinders the bond motions of the carbazole moiety and restrains the nonradiative decay, leading to a significant increase in the triplet-exciton lifetime. The prolonged triplet lifetime validates that enhanced structural rigidity can significantly improve the phosphorescence efficiency without affecting the heavy-atom effect, which provides a strategy for balancing phosphorescence lifetime and quantum yields.

DOI: 10.1103/PhysRevApplied.21.034037

I. INTRODUCTION

Organic room-temperature phosphorescent (RTP) emitters exhibit long-lived emissions, thus offering a wide range of applications, including data encryption [1,2], anticounterfeiting [2], sensing [3,4], and imaging [5,6]. These high-performance RTP emitters have a high phosphorescence quantum yield and long lifetimes [7], which are both related to the spin-flipped intersystem crossing (ISC). Nevertheless, according to the spin-selection rule, transitions between pure spin states of different multiplicity are generally forbidden. To achieve a high phosphorescence quantum yield, it is necessary to overcome this spin-forbidden nature via a large spin-orbit coupling (SOC), which is a relativistic phenomenon inducing the quantum mechanical mixing of states with different multiplicity [8]. Some feasible strategies, such as the introduction of heavy atoms (Br or I) [8,9] and heteroatoms (N, O, S) [10,11], were proposed for enhancing the SOC between singlet and triplet states. Previous studies have confirmed that the lone-pair electrons of the heteroatom increased the *n*-orbital composition during the transition process, which promoted ISC between the singlet and triplet states [12].

Nitrogen-hybridized carbazoles possess intrinsic weak triplet-state properties and are widely used to synthesize organic functional materials with ultralong phosphorescence [1,13–15]. Moreover, the planarized rigid structure of carbazole is favorable for restraining the nonradiative processes and stabilizing the triplet excitons [16,17]. Researchers proposed that carbazole could be easily functionalized at the 3-, 6-, or 9-positions and covalently linked to other molecular moieties [18]. In particular, the benzene-substituted derivative at the 9-position, 9-phenylcarbazole, has been widely used in the synthesis of functional molecules for organic light-emitting diodes [19,20] and optical sensing agents [21]. Orr-Ewing and co-workers reported the existence of a triplet state in 9-phenylcarbazole, and the corresponding ISC was

*yangyonggang@htu.edu.cn
†qinchaochao@htu.edu.cn
‡liuyufang2005@126.com

estimated to be 6900 ps by transient absorption (TA) spectroscopy [22]. Owing to a large SOC with increasing nuclear magnetic field, the introduction of halogen atoms can significantly promote the ISC efficiency and increase the population of triplet excitons [23,24]. Therefore, to investigate the application as the host in the organic light-emitting diode (OLED) materials, numerous derivatives based on 9-phenylcarbazole, such as heavy atoms and aromatic nucleus substitution of the carbazole or benzene moiety, were synthesized [22,25–27].

Although previous studies have confirmed the performance of 9-phenylcarbazole in RTP emitters, the exciton-decay dynamics of simple heavy-atom-substituted derivatives, especially the internal-space heavy-atom effect, has not been studied in depth. Although the heavy-atom effect improves the phosphorescence quantum yields, it significantly decreases the triplet lifetime [28,29], which is unfavorable for high-performance RTP emitters. Therefore, the balance between phosphorescence lifetime and quantum yields is pivotal to the development of organic phosphorescence emitters. Here, we focus on the heavy-atom effect of a single Br atom at different spatial positions (core or substituent group) on the forward ISC and phosphorescent properties. Different from a study of the relative positions of different bromine atoms [9], the influence of the spatial distance between a single bromine atom and the core carbazole moiety on the heavy-atom effect is studied in detail, rather than the mutual compensation effect between heavy atoms. The internal-space heavy-atom effects of commercially available 9-phenylcarbazole (**1**) and its bromine-substituted derivatives (**2**–**7**, Scheme 1) have been studied. Previous reports found that the spatial position of heavy atoms could significantly affect the spin-orbit coupling and change the rates of singlet–triplet-exciton transitions and triplet-exciton decay [30–32]. Lee *et al*. verified that the heavy atoms directly substituted on the core position in boron dipyrromethene generated more triplet excitons than at the *meso*-aryl position [31]. Similar conclusions were also drawn by Zhao and co-workers that a short distance between the heavy atom and fluorophore core led to efficient ISC [32]. To investigate the heavy-atom effect at different positions, the Br-substituted compounds at the *para*- (**2**), *meta*- (**3**), and *ortho*-positions (**4**) on the 9-phenyl moiety were considered, as well as derivatives **5** and **6** substituted directly at the carbazole core. The effects of heavy atoms at different positions on the ISC efficiency and triplet-exciton decay of 9-phenylcarbazole were investigated by femtosecond- (fs) and nanosecond- (ns) TA spectroscopy. The combination of fs- and ns-TA spectroscopy has been widely used to study the ultrafast excited-state dynamics of organic materials, which can provide real-time monitoring of the ISC process and exciton-decay processes [33,34]. Additionally, the changes to the molecular orbitals and spin-orbit couplings of these compounds are discussed using time-dependent density functional theory (TDDFT). Moreover, the prolonged lifetime of triplet excitons and efficient ISC of biphenyl-structured compound **7** were explored, followed by the analysis of the intrinsic photophysical mechanisms of the long-lived triplet state by theoretical simulations.

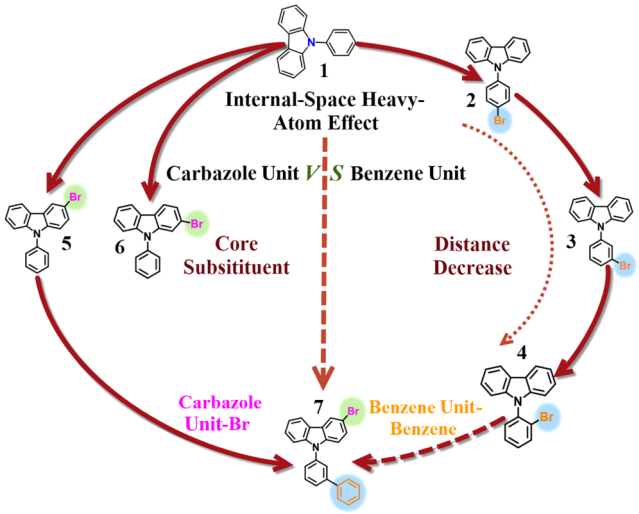

SCHEME 1. Chemical structure of 9-phenylcarbazole (**1**) and its Br-substituted derivatives (**2**–**7**).

II. EXPERIMENTAL DETAILS

A. Spectral measurements

All compounds and acetonitrile solvent with the highest available purity and spectrophotometric grade were purchased from Aladdin. All measurements were performed at room temperature [(20 ± 1)°C], except otherwise noted.

The absorption and fluorescence spectra were measured using a Cintra 2020 spectrophotometer (GBC, Australia) and FluoroMax-Plus spectrophotometer (HORIBA Japan), respectively. Each experiment was conducted in five replicates ($n = 5$). For oxygen-free measurements, solutions were bubbled with N2 for 30 min before measurements. For fs- and ns-TA spectroscopy, all the samples were thoroughly deoxygenated via nitrogen bubbling for 30 min and then sealed with parafilm prior to the measurements. The fs- and ns-TA spectra of the 9-phenylcarbazole derivatives were recorded using an Ultrafast Systems LLC and light source provided by a Helios pump-probe system. White-light-continuum probe pulses (390–600 nm) were produced by focusing an attenuated fraction of the fundamental 800-nm laser pulses (Coherent, 800 nm, 1 kHz, 7 mJ/pulse, 35 fs) onto a calcium fluoride crystal.

B. Theoretical simulations

The ground, singlet, and triplet excited states of the seven compounds were studied using DFT and TDDFT

[35–37] with the B3LYP functional and def2-TZVP basis sets [38–41] of the GAUSSIAN 16 program [42]. The solvation model based on density with acetonitrile solvent was added to ensure the simulation was close to the experimental environment [43]. The SOC constants between singlet and triplet states were calculated using the ORCA program [44]. The root-mean-square displacement (RMSD) was determined to measure geometric changes of these compounds in different states, which were visualized by the VMD program [41].The Hung-Rhys (HR) factors and reorganization energies analysis were simulated by the MOMAP program [45,46].

III. RESULTS AND DISCUSSION

Figure 1 shows the steady-state and TA spectra of compound **1** in acetonitrile solution. As shown in Figs. 1(a) and 1(b), the maximum absorption and fluorescence peaks of compound **1** are located at 337 and 360 nm, respectively, and a small Stokes shift of 23 nm is observed. For compound **1**, the calculated absorption energy of 323 nm (Table I) corresponds to the experimental absorption peak located at 337 nm, which confirms that the experimental absorption peak is attributable to the $S_0 \rightarrow S_1$ transition. The calculated fluorescence energy for the S_1 state (351 nm) is in agreement with the experimental values (360 nm). To monitor the exciton dynamic process in real time, the fs- and ns-TA spectra of compound **1** were measured in acetonitrile solution. In Fig. 1(c), the TA spectrum of compound **1** exhibits two signals located at 400 and 610 nm. As shown in Fig. 1(d), the signal at 610 nm reaches its maximum intensity within 1 ps, and then gradually decreases within 7 ns along with an increase of the pump-detection delay time. Meanwhile, the signal

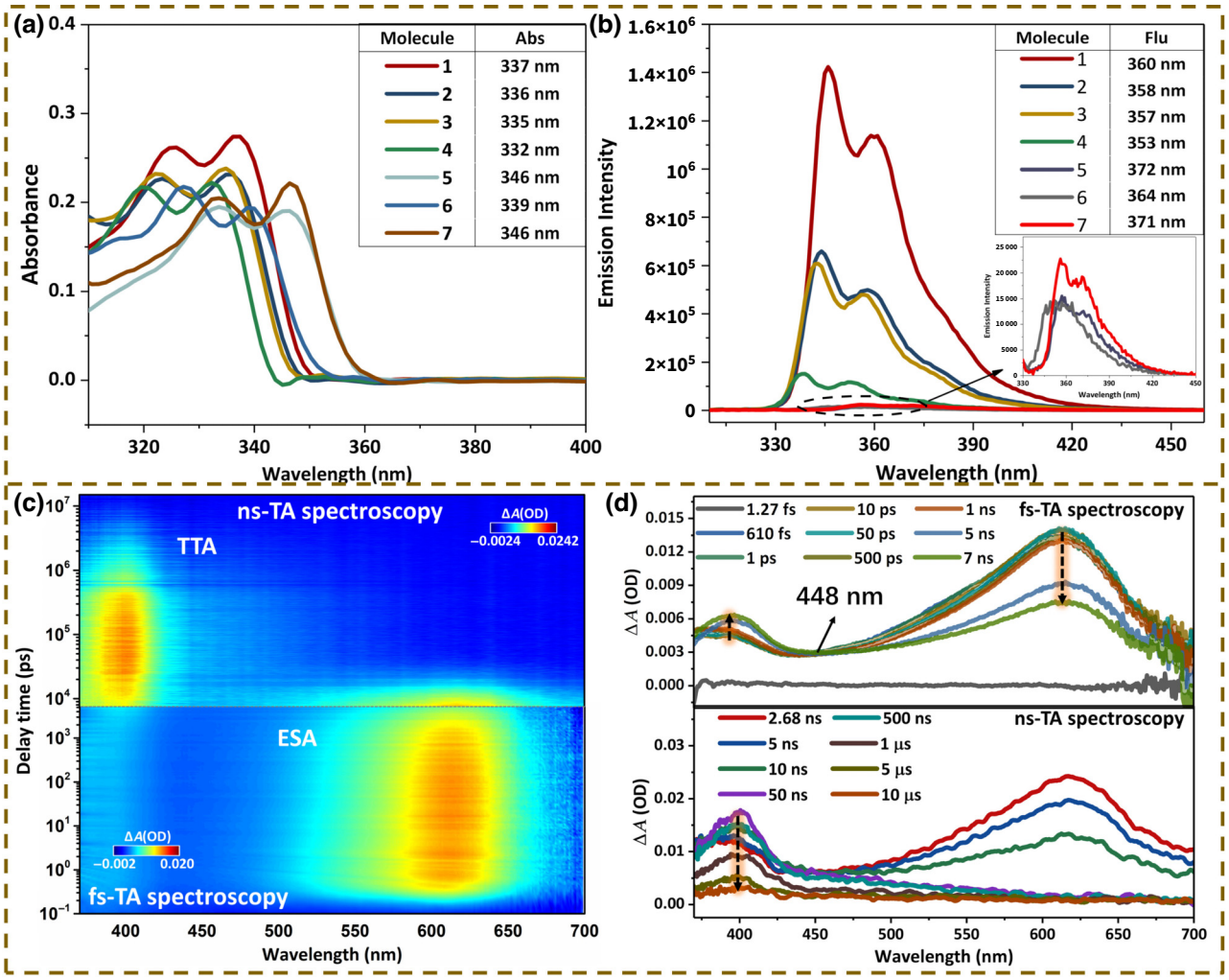

FIG. 1. (a) Experimental steady-state absorption and (b) emission spectra of 0.06-mM compounds **1**–**7** in acetonitrile solution. Excitation wavelength for the emission spectra of these compounds is 320 nm. Insets magnify the areas inside the shaded ellipses. Inset tables in panels (a),(b) are the maximum absorption and fluorescence peaks of compounds **1**–**7**, respectively. (c) Time-wavelength-dependent TA color maps of 1-mM compound **1** in acetonitrile solution pumped at 330 nm. Ordinate represents the delay time. (d) Time-resolved fs-TA (top) and ns-TA (bottom) spectra of 1-mM compound **1**. Ordinate represents the signal intensity. Each curve represents a TA signal at a specific pump-detection delay time.

intensity at 400 nm gradually increases, accompanying the appearance of an isosbestic point located at 448 nm. According to previous studies [33,47,48], the molecule is excited from the ground state to the singlet excited state by the pump pulse, and the singlet-singlet excited-state absorption (SESA) signal at 610 nm first appears in the TA spectrum. Subsequently, this SESA signal gradually decreases accompanied by a new increased positive signal (400 nm), and an isosbestic point (448 nm) appears in the middle of the two positive signals. The appearance of the isosbestic point confirms the occurrence of the exciton transition from the singlet state to the triplet state. Therefore, the signal at 610 nm is assigned to the SESA signal and the signal at 400 nm to the triplet-triplet absorption (T_1-T_n absorption) signal, which indicates the occurrence of ISC. And then the ns-TA spectrum in Fig. 1(d) shows that the T_1-T_n absorption signal gradually decays from 50 ns to 5 μs, reflecting the complete relaxation of the triplet-state exciton.

To gain further insights into the time-resolved exciton-relaxation dynamics, the kinetic data obtained from the fs- and ns-TA spectra of 9-phenylcarbazole are fitted using the SURFACE XPLORER software. All measured data are reserved for two significant figures. Figure 2(a) shows the decay-associated difference spectra and key time constants of the global fitting of fs-TA and ns-TA spectra. The reaction mechanism and coupled kinetic equations are shown in Fig. 7 of Appendix A. In the global fitting results, when the amplitude of the fitted lifetime component has the same sign as the signal intensity, it means that the characteristic signal is the decay of this lifetime component. On the contrary, when the amplitude and signal intensity have different signs, it represents an increase of this signal. The global fitting results show that the fs-TA spectrum of compound **1** has two spectral components, 138 fs and >7 ns, which are attributed to configurational relaxation induced by the solvation-stabilizing process and singlet-exciton relaxation, respectively. The spectral component of >7 ns reflects the decrease in the SESA signal (610 nm) and increase in the T_1-T_n absorption signal (400 nm), corresponding to the ISC lifetime. The global fitting of the ns-TA spectrum has two time components, 10 ns and 2.9 μs, which are assigned to the ISC lifetime and triplet-exciton relaxation, respectively. This ISC lifetime is consistent with the global fitting result ($\tau_{ISC} > 7$ ns) obtained by fs-TA spectroscopy. Moreover, to verify the global fitting results, single-wavelength kinetic fitting has been performed on the SESA and T_1-T_n absorption signals, as shown in Fig. 2(b). For the SESA signal, the τ_{rise} of 160 fs denotes the time required for the configurational relaxation and the τ_{decay} of >7 ns denotes the singlet-exciton lifetime. The SESA signal intensity does not decay to zero within the time window of 7 ns, indicating that the SESA lifetime of compound **1** exceeds the detection range of fs-TA spectroscopy. Therefore, the decay lifetime of the SESA signal is fitted as >7 ns in the kinetic fitting

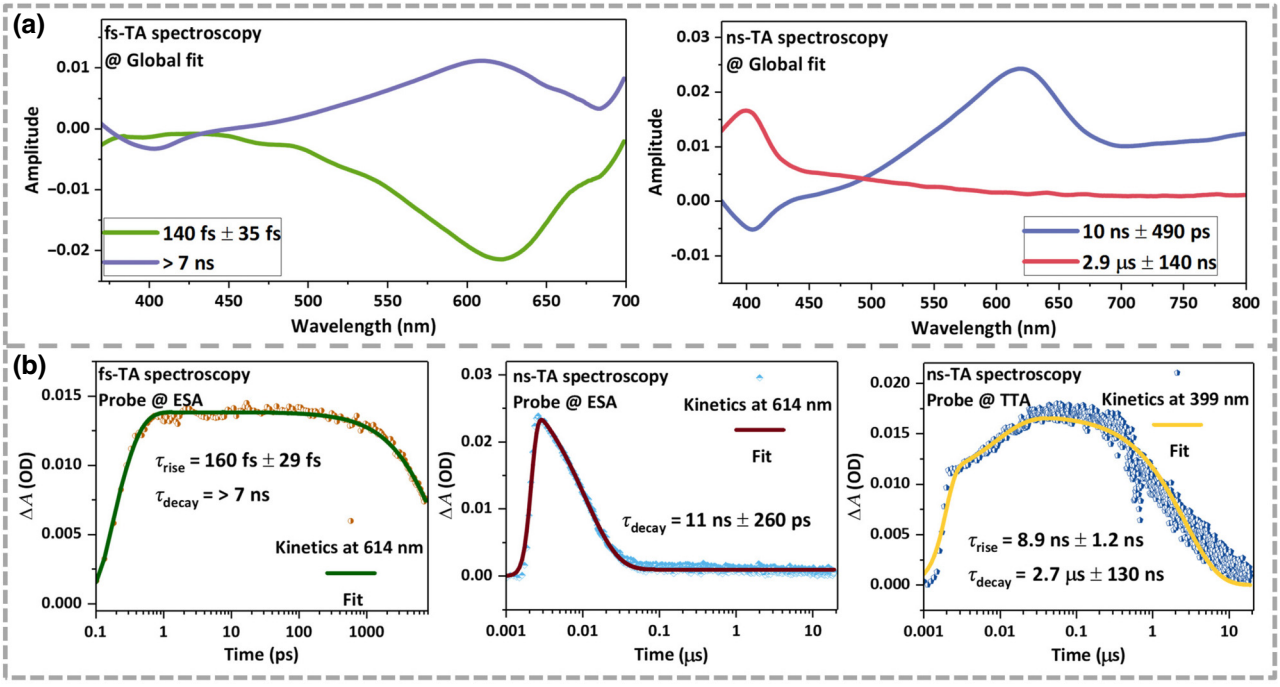

FIG. 2. (a) Decay-associated difference spectra (DADS) obtained by global fitting analysis of compound **1** by fs-TA (left) and ns-TA spectroscopy (right). (b) Kinetic fitting of the SESA and T_1-T_n absorption signals for compound **1** in fs-TA (left) and ns-TA spectra (middle and right).

of the fs-TA spectra. In ns-TA spectroscopy, the decay of the singlet exciton is monoexponential, as expected for a monomolecule in fs-TA spectroscopy. The kinetic fitting shows that the ISC lifetime and triplet-exciton relaxation are 8.9 ns and 2.7 μs, respectively, for the T_1-T_n absorption signal, which agrees well with the global fitting results (10 ns and 2.9 μs). Accordingly, the lifetimes of ISC and triplet-exciton relaxation of compound **1** are about 10 ns and 2.8 μs in acetonitrile solution.

The influence of heavy atoms, especially substituted at different spatial positions, on the triplet-state quantum yield and lifetime has been considered. The different internal-space heavy-atom effects, including in the 9-phenyl moiety (**2**, **3**, and **4**) and carbazole moiety (**5** and **6**), have been studied for the steady-state and TA spectra. First, the spectral dynamics of Br-substituted benzene-ring derivatives are discussed. As shown in Fig. 1(b), the fluorescence peaks of substituted derivatives in the *para*- (**2**), *meta*- (**3**), and *ortho*-positions (**4**) are located at 358, 357, and 353 nm, respectively. The fluorescent intensities of the three compounds decrease compared to the heavy-atom-free 9-phenylcarbazole, indicating that the phosphorescence efficiency could be enhanced with the introduction of the Br atom. Figures 3(a)–3(c) show the fs- and ns-TA spectra of compounds **2**, **3**, and **4**, respectively. For compound **2**, the fs- and ns-TA spectra show the SESA and T_1-T_n absorption signals. The SESA signal intensity reaches its maximum value within 1 ps and then gradually decays within 10 ns, accompanying the rise of the T_1-T_n absorption signal. The isosbestic point at 426 nm exhibits the occurrence of an excitonic transition from the singlet state to the triplet state. Subsequently, the T_1-T_n absorption peak of triplet exciton disappears in 1 μs with time evolution. Similarly, both *meta*-substituted compound **3** and *ortho*-substituted compound **4** show two bands corresponding to the SESA and T_1-T_n absorption signals. In the time-evolution TA spectra, the SESA and T_1-T_n absorption peaks of compound **3** gradually disappear within 5 ns and 1 μs respectively, and those of compound **4** disappear within 3 and 500 ns, respectively. With the shortening

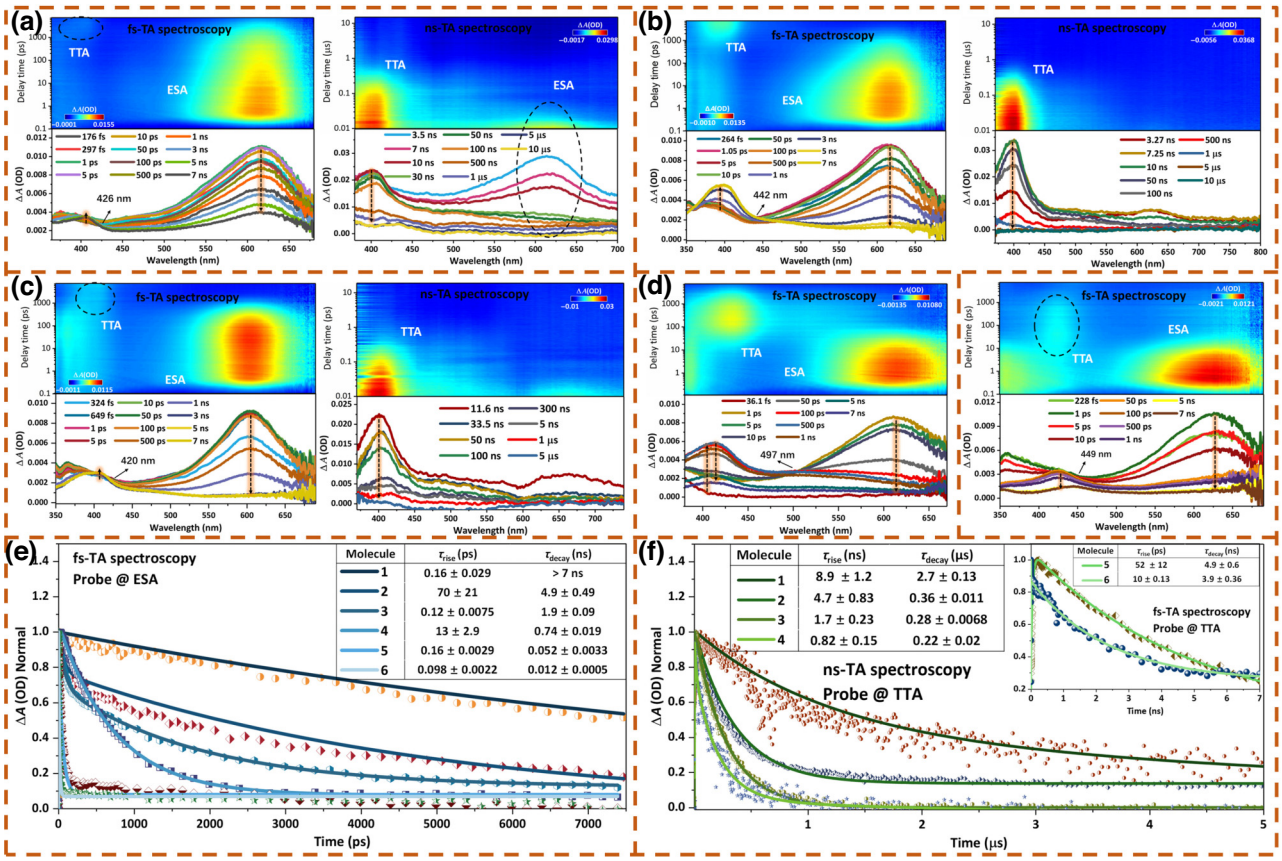

Molecule	τ_{rise} (ps)	τ_{decay} (ns)
1	0.16 ± 0.029	> 7 ns
2	70 ± 21	4.9 ± 0.49
3	0.12 ± 0.0075	1.9 ± 0.09
4	13 ± 2.9	0.74 ± 0.019
5	0.16 ± 0.0029	0.052 ± 0.0033
6	0.098 ± 0.0022	0.012 ± 0.0005

Molecule	τ_{rise} (ns)	τ_{decay} (μs)
1	8.9 ± 1.2	2.7 ± 0.13
2	4.7 ± 0.83	0.36 ± 0.011
3	1.7 ± 0.23	0.28 ± 0.0068
4	0.82 ± 0.15	0.22 ± 0.02

Molecule	τ_{rise} (ps)	τ_{decay} (ns)
5	52 ± 12	4.9 ± 0.6
6	10 ± 0.13	3.9 ± 0.36

FIG. 3. (a)–(c) Time-wavelength-dependent fs-TA and ns-TA color maps of 1-mM solutions of compounds **2**, **3**, and **4**, respectively. (d),(e) Time-wavelength-dependent fs-TA color maps of 1-mM solutions of compounds **5** and **6**, respectively. All the color maps are measured in acetonitrile solution and pumped at 330 nm. (f) Normalized fs-TA kinetic curves of the SESA bands for compounds **1**–**6** in acetonitrile. (g) Normalized ns-TA kinetic curves of the T_1-T_n absorption bands for compounds **1**–**6** in acetonitrile. Dots and solid lines represent experimental values and fitted values, respectively. Inset tables in panels (f),(g) are the time components of fs- and ns-TA spectroscopy for different molecules obtained by double-exponential kinetic fitting.

of the spatial distance between the bromine atom and carbazole moiety (*ortho*-position < *meta*-position < *para*-position), the 9-phenylcarbazole derivatives exhibit faster ISC, inducing a more efficient triplet exciton. Second, to verify the aforementioned conclusion, the exciton dynamics of derivatives substituted in the carbazole moiety (**5** and **6**) was investigated. As shown in Fig. 1(b), the fluorescence peaks of compounds **5** and **6** are almost completely quenched compared to the derivatives substituted in the benzene ring. This indicates that compounds **5** and **6** might have low fluorescence quantum yields and high phosphorescence efficiencies. The fs-TA spectra in Figs. 3(d) and 3(f) show that the SESA peaks of compounds **5** and **6** disappear at 100 and 50 ps, respectively; this faster than those of compounds **2**, **3**, and **4**. Moreover, the T_1-T_n absorption signal intensities of compounds **5** and **6** decrease to zero within 7 ns, indicating that the triplet excitons of both compounds have completely decayed. These results demonstrate that the ISC and triplet-exciton lifetimes of derivatives with heavy-atom substitution in the carbazole moiety are shorter than those substituted in the benzene ring.

To further visualize the exciton dynamics in different substituted derivatives, the kinetic curves of SESA and T_1-T_n absorption signals of compounds **1**–**6** are extracted and presented in Figs. 3(f) and 3(g). Notably, with a decreasing distance between the heavy atom and the core carbazole moiety, the kinetic curves of the SESA and T_1-T_n absorption signals become steeper, indicating the shortening of the corresponding decay time for singlet and triplet excitons. The kinetic fitting of each curve is performed and shown in the inset tables. The ISC lifetime follows the order of heavy-atom-free compound **1** (>7 ns) > *para*-position-substituted compound **2** (4.9 ns) > *meta*-position-substituted compound **3** (1.9 ns) > *ortho*-position-substituted compound **4** (0.74 ns) > carbazole-substituted compounds **5** and **6** (0.052 ns and 0.012 ns). The corresponding T_1-T_n absorption lifetimes exhibit the same order, **1** (2.7 μs) > **2** (0.36 μs) > **3** (0.28 μs) > **4** (0.22 μs) > **5** (4.9 ns) > **6** (3.9 ns), showing that the enhancement of the heavy-atom effect leads to rapid decay processes of triplet excitons. The decay-associated difference spectra and key time constants of the global fitting are shown in Figs. 8–12 of Appendix A. Similarly, the decay lifetimes of the corresponding singlet and triplet excitons gradually decrease as the distance shortens between the bromine atom and the carbazole moiety, which agrees well with the kinetic fitting results. These results show that the bromine-substituted 9-phenylcarbazole derivatives have more efficient ISCs and shorter relaxation lifetimes of the triplet exciton. Moreover, when bromine is directly substituted onto the core carbazole of the 9-phenylcarbazole, a greater heavy-atom effect and increased triplet exciton can be induced.

Theoretical calculations are performed to gain further insights into the heavy-atom effect of 9-phenylcarbazole derivatives, as listed in Fig. 4 and Tables II–VIII of Appendix B. In the FMOs, the electron density of the highest occupied molecular orbital (HOMO) for the S_1 and T_1 states is distributed over the entire molecule, which transfers to the carbazole moiety after the transition to the lowest unoccupied molecular orbital (LUMO). These transfers show that the S_1 and T_1 states of the six compounds are obvious charge-transfer states, which bridge the two states and promote their ISC. As shown in Tables II–VIII of Appendix B, all six 9-phenylcarbazole derivatives have the approximate HOMO → LUMO transition configuration in the singlet and triplet states. Similar transition configurations indicate that these six compounds have a possible ISC channel. Moreover, the orbital types in the S_1 and T_1 states of heavy-atom-free compound **1** are assigned to the $\pi \rightarrow \pi^*$ transition. For the bromine-substituted derivatives compounds **2**–**6**, the lone-pair electrons on the bromine atom increase the *n*-orbital composition and favor the exciton transition from the singlet state to the triplet state, resulting in an efficient ISC. Moreover, for compound **1**, the calculated energies for T_1, T_2, T_3, and T_4 are 3.10, 5.67, 6.18, and 6.72 eV, respectively (Table IX). In the TA spectrum, the T_1-T_n absorption signal located at 410 nm for compound **1** is attributed to the transition from the T_1 state to the T_3 state (3.08 eV, 403 nm), which then decays to the T_1 state by internal conversion. For the other six molecules, the energy maps between the T_1 and T_3 states are calculated as 3.08 (compound **2**), 3.08 (compound **3**), 3.10 (compound **4**), 3.05 (compound **5**), 3.04 (compound **6**), and 3.05 eV (compound **7**). These results show that the T_1-T_n absorption signals of all the molecules are attributed to the transition from the T_1 state to the T_3 state.

Spin-orbit coupling arises from the interaction of the spin magnetic moment of an electron and the magnetic field resulting from the apparent motion of the nucleus [8]. The introduction of a heavy atom enhances the nuclear magnetic field, leading to an increase in spin-orbit coupling. Herein, the SOC constants are calculated and presented in Fig. 4(b). For free-heavy-atom compound **1**, the SOC constants (ξ) between the S_1 and T_1 states are calculated to be 0.013 cm^{-1}. When the Br atoms are introduced, $\xi(S_1\text{-}T_1)$ is enhanced and with the decrease in the spatial distance between the bromine atom and carbazole moiety, this value changes from 0.033 cm^{-1} in the *para*-position to 0.11 cm^{-1} in the *meta*-position and 0.16 cm^{-1} in the *ortho*-position. Furthermore, with bromine substitution on the carbazole core, compounds **5** and **6** have larger SOC values (0.33 and 1.7 cm^{-1}, respectively) than those of compounds **2**–**4**. These results indicate that for 9-phenylcarbazole molecules, the shortening of the spatial distance induces a stronger heavy-atom effect, resulting in an enhancement of ISC with high efficiency and triggering a high population of triplet excitons. The calculated

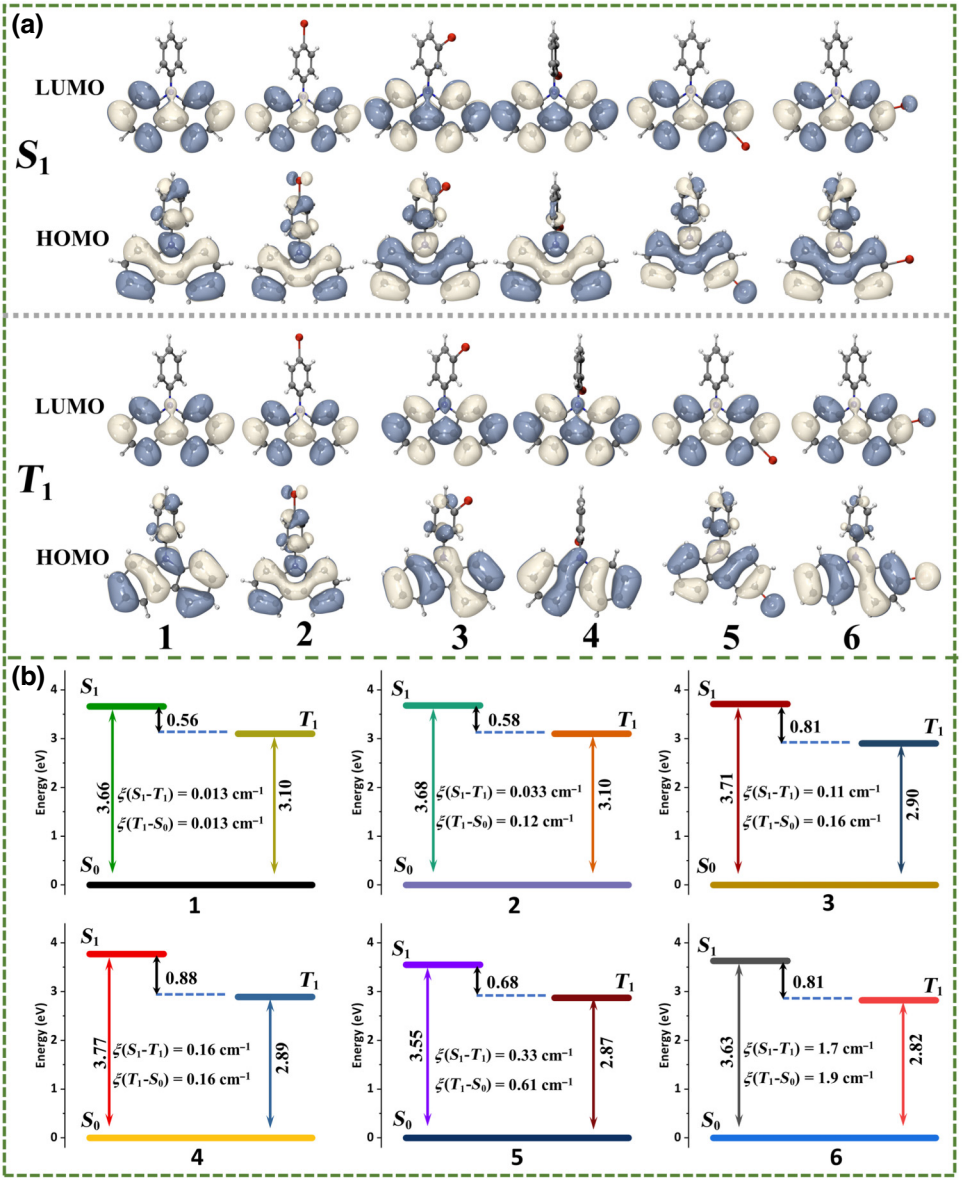

FIG. 4. (a) Frontier molecular orbits (FMOs) of compounds **1**–**6** based on the S_1 and T_1 configurations. (b) Calculated energy diagrams of a three-level model for compounds **1**–**6**. $\xi(S_1\text{-}T_1)$ and $\xi(T_1\text{-}S_0)$ represent the spin-orbit coupling constants between singlet and triplet states, respectively.

SOC values between T_1 and S_0 states show a similar trend, indicating that the internal heavy-atom effect has a significant influence on both the rate of ISC_{S1-T1} and ISC_{T1-S0} related to triplet-exciton decay. Moreover, the ISC rate for the $S_1 \rightarrow T_1$ transition is calculated, as shown in Table X. The calculations show that the ISC rate between the S_1 and T_1 states of compound **1** is 1.9×10^4 s^{-1}. After Br atoms are introduced into the 9-phenyl moiety, this value changes from 2.4×10^4 s^{-1} in compound **2** to 7.1×10^4 s^{-1} in compound **3** and to 7.0×10^5 s^{-1} in compound **4**. For Br substitution on the carbazole core, compounds **5** and **6** have larger ISC rates (2.1×10^6 and 8.6×10^7 s^{-1}, respectively) than those of compounds **2**–**4**. The shortening of the spatial distance induces an efficient ISC rate, which is consistent with the SOC values. These results further confirm that the shortening of the spatial distance induces a stronger heavy-atom effect.

The triplet-state lifetime is an important index to evaluate the properties of organic phosphorescent molecules. The aforementioned results proved that the introduction of bromine atoms into the 9-phenylcarbazole compounds led to a significant decrease in the triplet-exciton lifetime. Therefore, based on compound **5**, biphenyl-structured compound **7** was investigated for its prolonged triplet-exciton process. Figure 5(a) shows the fs and ns-TA spectra of compound **7** in acetonitrile solution. The fs-TA

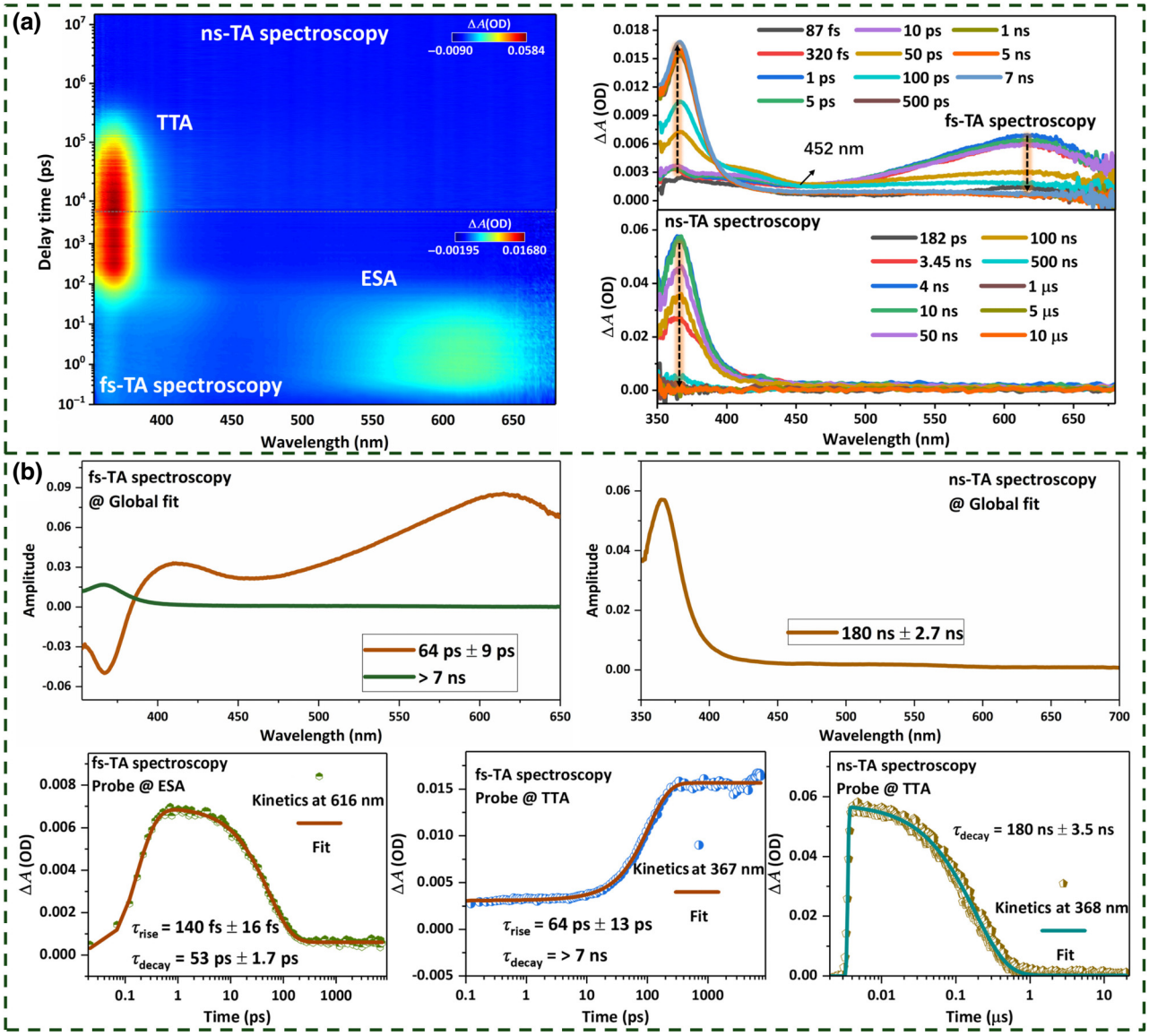

FIG. 5. (a) TA spectra of 1-mM compound **7** in acetonitrile solution pumped at 330 nm. (b) Global fitting analysis (top) and kinetic fitting (bottom) of compound **7** by fs-TA and ns-TA spectroscopy.

spectrum shows that compound **7** also has SESA and T_1-T_n absorption signals, accompanying the isosbestic point at 452 nm. The time-evolution spectral curve shows that the SESA peak of compound **7** completely decays within 50 ps, which is similar to that of compound **5**. However, the T_1-T_n absorption signal has an obvious characteristic peak in 100 ns, which indicates that the compound **7** has a longer triplet-exciton lifetime. To visually reflect the exciton-decay lifetime, global fitting and kinetic fitting were performed, as displayed in Fig. 5(b). The global fitting shows that the fs-TA spectrum of compound **7** has two spectral components, 64 ps and >7 ns, which correspond to the exciton-decay time of the singlet and triplet states, respectively. In the ns-TA spectrum, the spectral component at 180 ns is assigned to the relaxation process of the triplet exciton. Moreover, the kinetic fitting of the SESA signal exhibits two lifetime components, 140 and 53 ps, which represent the lifetime of the configurational relaxation (τ_{rise}) and singlet-exciton decay (τ_{decay}). Additionally, the rise time of the T_1-T_n absorption signal is fitted as 64 ps, implying that the ISC time of compound **7** is about 60 ps. For ns-TA spectroscopy, the decay lifetime of the T_1-T_n absorption signal is fitted as 180 ns, which is approximately 40 times longer than the triplet-exciton lifetime of compound **5**. These results demonstrate that the 9-phenylcarbazole derivative with a biphenyl structure, compound **7**, has a high ISC efficiency and it can significantly improve the triplet-exciton lifetime.

To better explain the longer triplet-exciton lifetime of compound **7**, theoretical simulations were performed, and

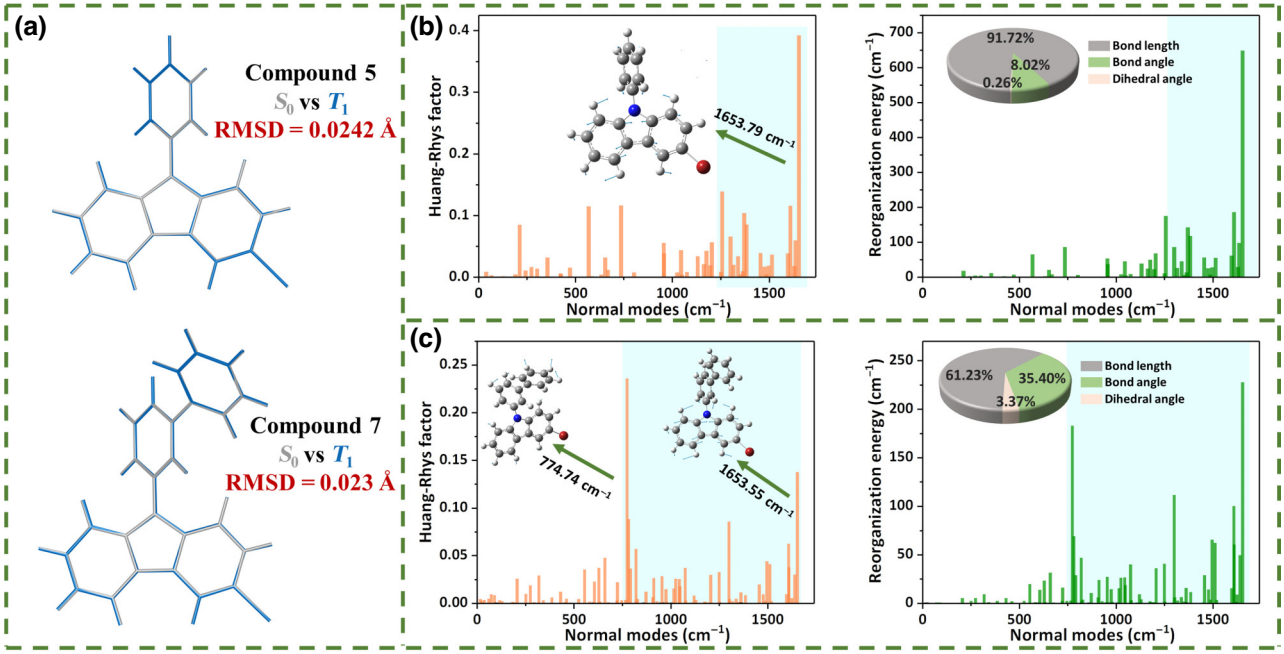

FIG. 6. (a) Geometry comparisons of compounds **5** (top) and **7** (bottom) between S_0 (silver) and T_1 (blue) states. (b),(c) Calculated HR factors and reorganization energies versus the normal-mode frequencies of compounds **5** and **7** in acetonitrile solution, respectively. Inset pie charts represent the corresponding contribution ratios to total reorganization energies from the bond length, bond angle, and dihedral angle.

the corresponding results are presented in Fig. 6. The calculated SOC between the S_1 and T_1 states of compound **7** (0.3528 cm^{-1}) is close to that of compound **5** (0.3320 cm^{-1}), indicating that the biphenyl group has a slight effect on the internal-space heavy-atom effect and ISC. All the photophysical properties are closely related to molecular conformations. To quantitatively measure the geometric changes between different states, the RMSD is calculated for compounds **5** and **7** by

$$\mathrm{RMSD} = \sqrt{\frac{1}{N}\sum_{i}^{N_{\mathrm{atom}}}\left[(x_i - x_i')^2 + (y_i - y_i')^2 + (z_i - z_i')^2\right]},$$

where i cycles all atoms. x_i, y_i, and z_i represent the x-, y-, and z coordinates, respectively, of the ith atom in the first structure (S_0 state in this part). x_i', y_i', and z_i' represent the x-, y-, and z coordinates, respectively, of the ith atom in the second structure (T_1 state in this part).

The RMSDs between the S_0 and T_1 states of compounds **5** and **7** are calculated to be 0.0242 and 0.023 Å, respectively, implying that the structural change to compound **5** is larger than that of compound **7** during the triplet-exciton dynamic process. Moreover, the HR factor and reorganization energy are two effective parameters to describe nonradiative consumption [49,50]; these are calculated and shown in Figs. 6(b) and 6(c). In Fig. 6(b), the representative large HR factor of compound **5** is 0.39 (1653.79 cm^{-1}), corresponding to the bond vibration of the carbazole moiety, as shown in the insets. For compound **7**, the HR factor of this vibrational mode decreases to 0.14, confirming that the bond motions of the carbazole moiety in the high-frequency regions are hindered by the biphenyl structure. In Fig. 6(c), the reorganization energies versus the normal-mode frequencies show that the reorganization energies of compounds **5** and **7** at 1653.79 cm^{-1} are 648.6 and 227.63 cm^{-1}, respectively, and the sums of the reorganization energies in the high-frequency regions of compound **5** are larger than that of compound **7**. To better illustrate the nonradiative intensity, the total reorganization energies of the two compounds are calculated. The total reorganization energy of compound **7** decreases to 1654 cm^{-1} compared to that of compound **5** (2433 cm^{-1}). This decrease indicates that the biphenyl structure significantly inhibits the nonradiative decay of the triplet exciton, leading to a significant increase of the triplet-exciton lifetime of compound **7**. Furthermore, the calculated reorganization energies contributed from the bond length, bond angle, and dihedral angle show that the bond-length contribution to the reorganization energies plays the major part in the two compounds. However, the ratio of bond lengths decreased from 91.72% (**5**) to 61.23% (**7**), indicating that the biphenyl structure inhibited the vibration of bond lengths, thereby significantly restraining the nonradiative decay. Thus, the theoretical simulation results reasonably explain the long triplet state of compound **7**,

suggesting that energy dissipation via vibration decay can be suppressed due to structural modification.

IV. CONCLUSIONS

Here, the internal-space heavy-atom effects on the phosphorescence behaviors of 9-phenylcarbazole derivatives were studied by TA spectroscopy and theoretical simulations. For heavy-atom-free compound **1**, the T_1-T_n absorption signal (400 nm) gradually increased with the decreasing SESA signal (610 nm), accompanied by the appearance of an isosbestic point located at 448 nm, which indicated the occurrence of ISC from the singlet state to the triplet state. The lifetimes of ISC and triplet-exciton relaxation of compound **1** were about 10 ns and 2.8 μs, respectively, in acetonitrile solution. For Br-substituted derivatives, the TA spectroscopy results showed that the ISC efficiency order was carbazole-substituted derivatives (**5** and **6**, 0.052 and 0.012 ns, respectively) > *ortho*-position-substituted derivative (**4**, 0.74 ns) > *meta*-position-substituted derivative (**3**, 1.9 ns) > *para*-position-substituted derivative (**2**, 4.9 ns) > heavy-atom-free derivative (**1**, > 7 ns). Therefore, with the shortening of the spatial distance between the bromine atom and the carbazole moiety, the 9-phenylcarbazole derivatives exhibited faster ISC. Theoretical calculations indicated that the increase in *n*-orbital composition was induced by lone-pair electrons on the bromine atom and the enhancement of $\xi(S_1\text{-}T_1)$ induced the enhancement of ISC, thereby triggering a highly efficient triplet exciton. However, the triplet-exciton decay of these derivatives gradually decreased with the enhancement of ISC efficiency. Therefore, based on compound **5**, biphenyl-structured compound **7** was investigated for its exciton-transition process. For compound **7**, the measured lifetime of the triplet exciton was 183.3 ns, which was approximately 40 times longer than that of compound **5**. The calculated reorganization energies of compound **7** (1654 cm^{-1}) were much smaller than that of compound **5** (2433 cm^{-1}), showing a significant decrease in the nonradiative decay of compound **7**. Additionally, the decrease in the HR factor confirmed that the bond-length motions of the carbazole moiety in the high-frequency regions were hindered by the biphenyl structure. These results demonstrate that the biphenyl structure inhibits the vibration of bond lengths and thereby significantly restrains nonradiative decay, leading to the prolongation of the triplet-exciton-decay process.

ACKNOWLEDGMENTS

This work is supported by the National Natural Science Foundation of China (Grants No. 11974103, No. 11274096, No. 12074104, and No. 11804084), the Henan Province University Science and Technology Innovation Talent Support Plan (Grant No. 21HASTIT019), the Henan Province Science and Technology Research and Development Plan Joint Fund (225200810039), the Program for Innovative Research Team (in Science and Technology) of University of Henan Province (Grant No. 13IRTSTHN016). The calculations for this work were supported by The High Performance Computing Center of Henan Normal University.

APPENDIX A: GLOBAL FITTING AND KINETIC FITTING

In Fig. 7, we use coupled kinetic equations to fit the time profile in the kinetic analysis. The S_0, S_1', S_1, S_n, T_1, and T_n states correspond to the ground state, the high vibrational level of the first excited-singlet state, the low vibrational level of the first excited-singlet state, the high excited-singlet state, the first triplet state, and the high triplet state, respectively. The coupled kinetic equations of these compounds are given by

$$\frac{d[S'_1]}{dt} = -\frac{1}{\tau_1}[S'_1] + \sigma_a I_{\text{pump}}(t)[S_0],$$

$$\frac{d[S_1]}{dt} = -\left(\frac{1}{\tau_2} + \frac{1}{\tau_3}\right)[S_1] + \frac{1}{\tau_1}[S'_1],$$

$$\frac{d[T_1]}{dt} = -\frac{1}{\tau_4}[T_1] + \frac{1}{\tau_3}[S_1],$$

$$\frac{d[S_0]}{dt} = \frac{1}{\tau_2}[S_1] + \frac{1}{\tau_4}[T_1] - \sigma_a I_{\text{pump}}(t)[S_0],$$

where $[S_0]$, $[S_1]$, and $[T_1]$ represent the relative population of the ground state, first excited-singlet state, and first triplet state. σ_a is the photoabsorption cross section and $I_{\text{pump}}(t)$ is the pump laser intensity. $1/\tau_2$, $1/\tau_3$, and $1/\tau_4$ represent the transition rates of S_1-S_0, S_1-T_1, and T_1-S_0. $1/\tau_1$ represents the vibration-relaxation rates.

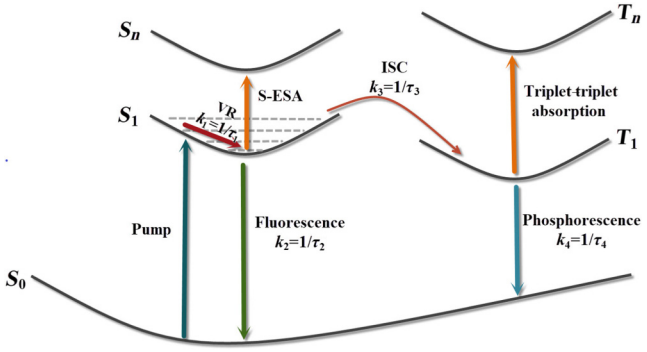

FIG. 7 Reaction mechanism of these compounds.

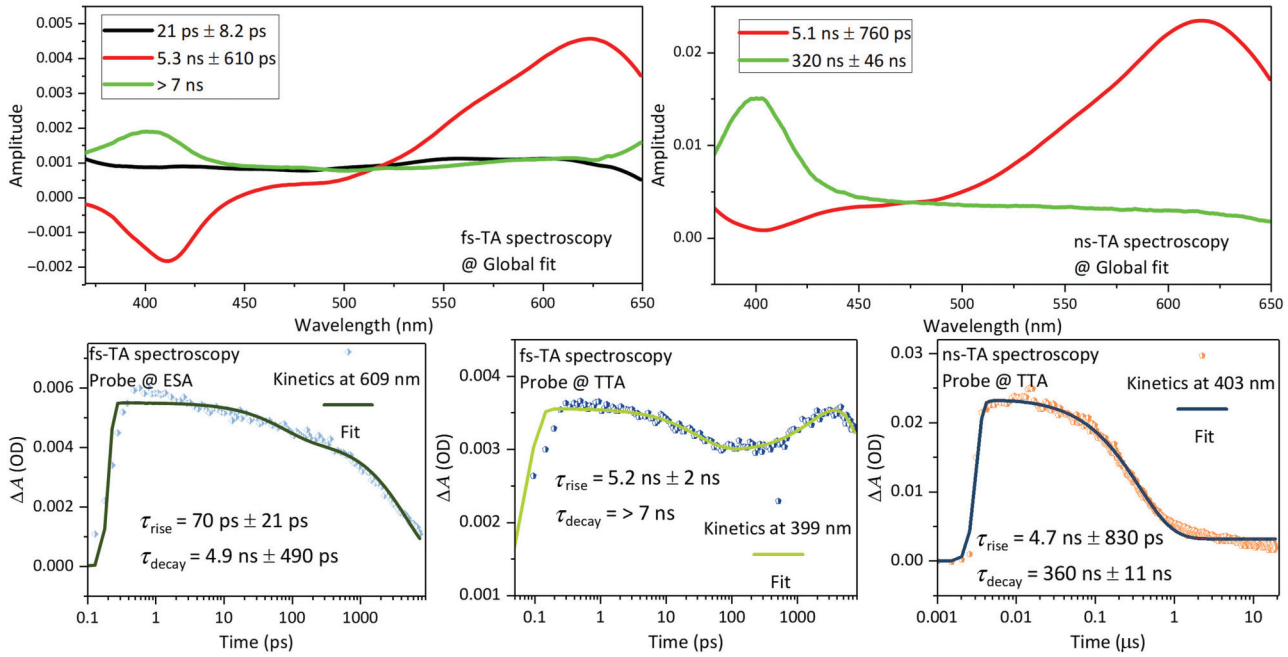

FIG. 8. Top, DADS obtained by global fitting analysis of compound **2** by fs-TA (left) and ns-TA spectroscopy (right). Bottom, kinetic fitting of the SESA and T_1-T_n absorption signals for compound **2** by fs-TA and ns-TA spectroscopy.

In Fig. 8, the global fitting shows that the fs-TA spectroscopy of compound **2** has three spectral components, 21 ps, 5.3 ns, and >7 ns, which correspond to the configurational relaxation, singlet exciton decay, and triplet exciton decay, respectively. In the ns-TA spectroscopy, the spectral components of 5.3 ns and 320 ns are assigned to the relaxation process of singlet and triplet states, respectively. Moreover, the kinetic fitting of the SESA signal exhibits two lifetime components, 70 ps and 4.9 ns, which represent the lifetimes of the configurational relaxation and singlet exciton decay.

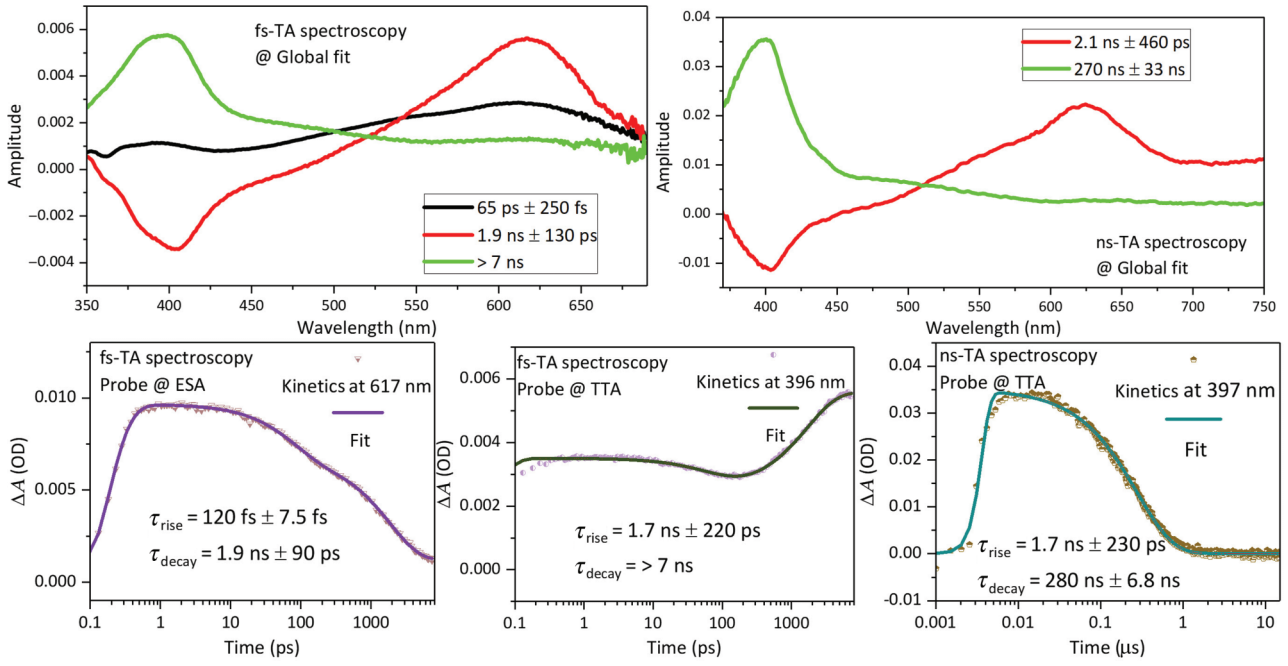

FIG. 9. Top, DADS obtained by global fitting analysis of compound **3** by fs-TA and ns-TA spectroscopy. Bottom, kinetic fitting of the SESA and T_1-T_n absorption signals for compound **3** by fs-TA and ns-TA spectroscopy.

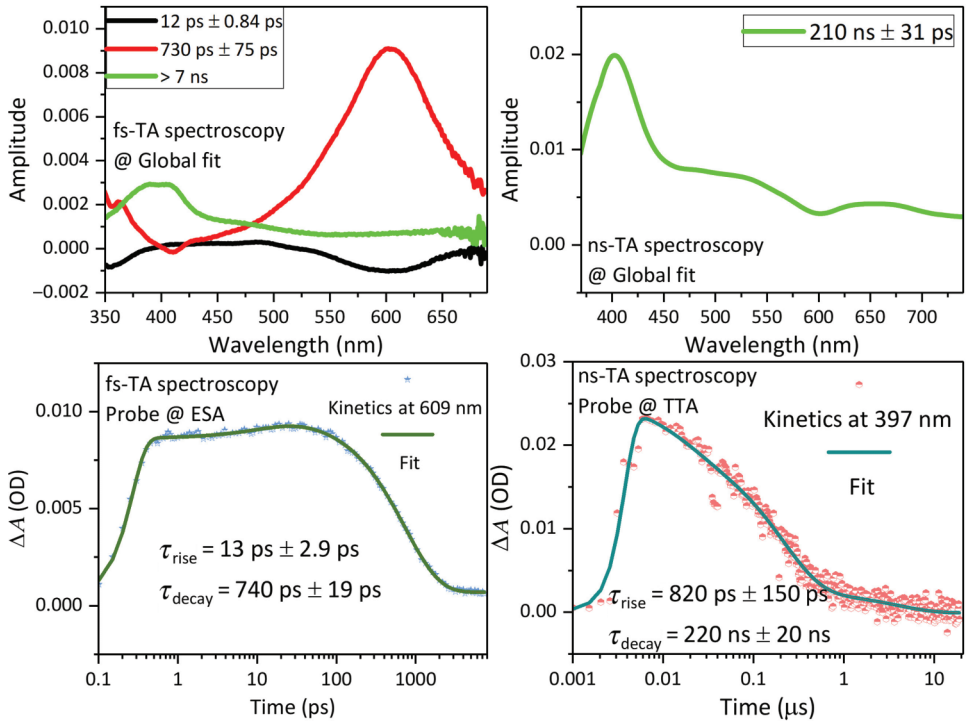

FIG. 10. Top, DADS obtained by global fitting analysis of compound **4** by fs-TA and ns-TA spectroscopy. Bottom, kinetic fitting of the SESA and T_1-T_n absorption signals for compound **4** by fs-TA and ns-TA spectroscopy.

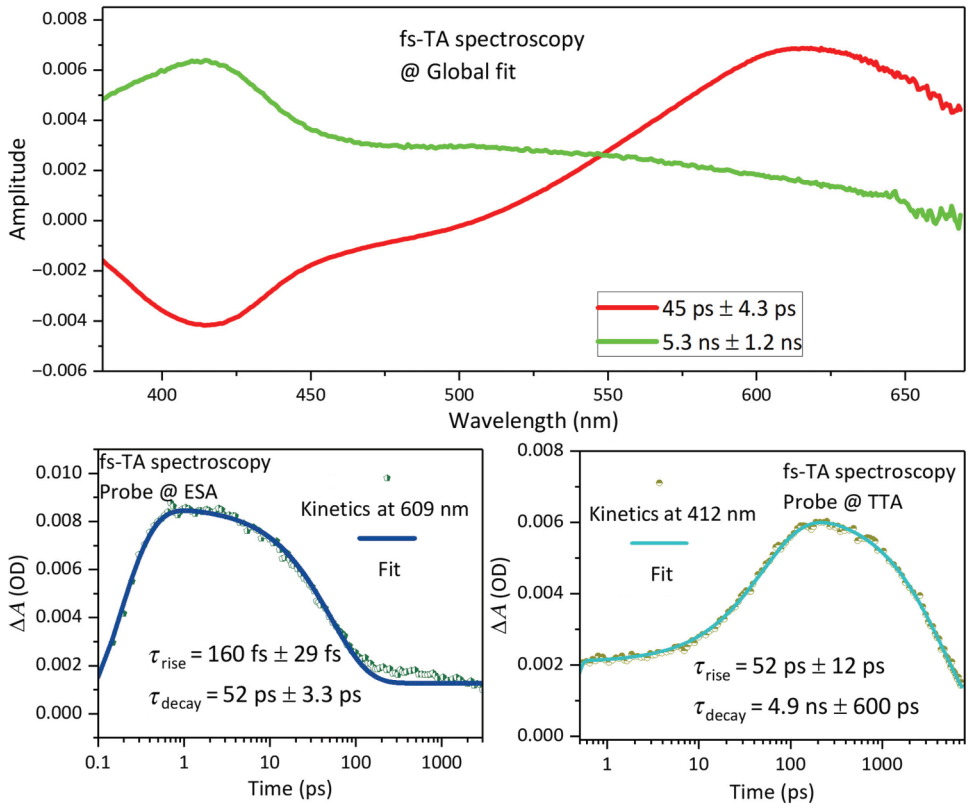

FIG. 11. Top, DADS obtained by global fitting analysis of compound **5** by fs-TA spectroscopy. Bottom, kinetic fitting of the SESA and T_1-T_n absorption signals for compound **5** by fs-TA spectroscopy.

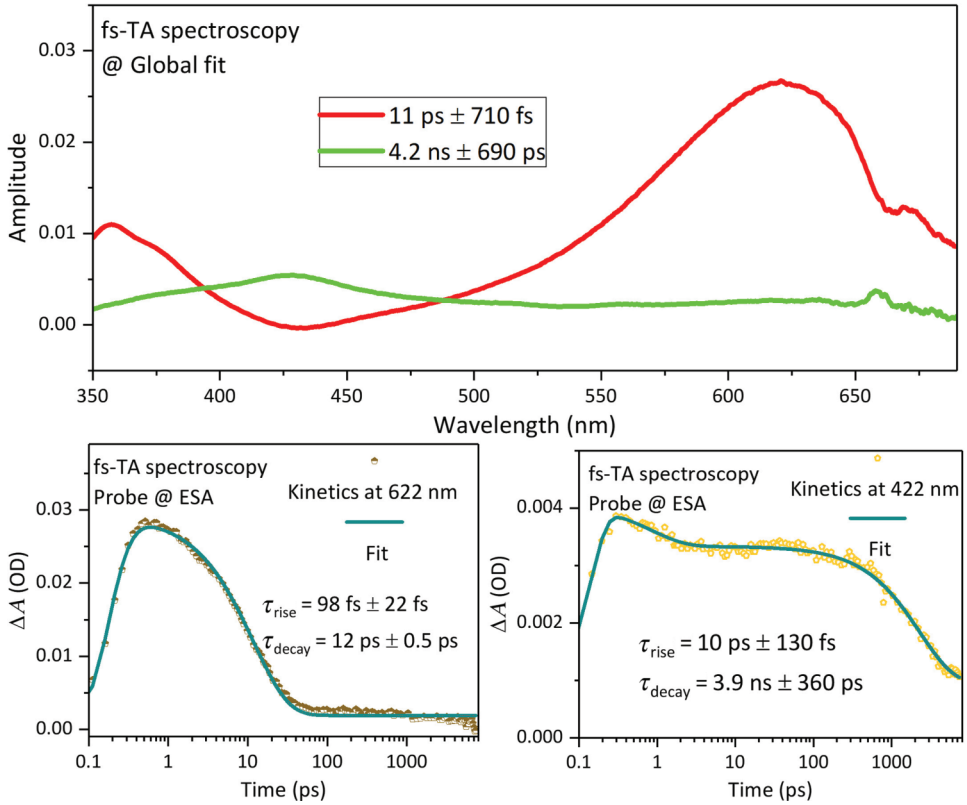

FIG. 12. Top, DADS obtained by global fitting analysis of compound **6** by fs-TA spectroscopy. Bottom, kinetic fitting of the SESA and T_1-T_n absorption signals for compound **6** by fs-TA spectroscopy.

In addition, the rise time of the T_1–T_n absorption signal is fitted as 5.2 ns, implying that the ISC time of compound **2** is approximately 5 ns. For ns-TA spectroscopy, the decay lifetime of T_1–T_n absorption signal is fitted as 360 ns.

As shown in Fig. 9, the global fitting in the fs-TA spectroscopy shows that compound **3** has three spectral components, 65 ps, 1.9 ns, and >7 ns, which correspond to the configurational relaxation, singlet exciton decay, and triplet exciton decay, respectively. In the ns-TA spectroscopy, the spectral components of 2.1 ns and 270 ns are assigned to the relaxation process of singlet and triplet states, respectively. Moreover, for the SESA signal, τ_{decay} (1.9 ns) in the kinetic fitting represents the lifetime of singlet exciton decay. The rise time of the T_1–T_n absorption signal is fitted as 1.7 ns, implying that the ISC time of compound **3** is approximately 2 ns. In the ns-TA spectroscopy, the decay lifetime of T_1–T_n absorption signal is fitted as 280 ns.

In Fig. 10, the global fitting shows that the fs-TA spectroscopy of compound **4** has three spectral components, 12 ps, 730 ps, and >7 ns, which correspond to the configurational relaxation, singlet exciton decay, and triplet exciton decay, respectively. In the ns-TA spectroscopy, the spectral component of 210 ns is assigned to the relaxation process of the triplet state. Moreover, in the kinetic fitting, the exciton decay of SESA and T_1–T_n absorption signals are fitted as 740 ps and 220 ns, respectively.

In Fig. 11, the two spectral components (45 ps and 5.3 ns) in the global fitting of compound **5** correspond to the exciton decay times of singlet and triplet states, respectively. Moreover, τ_{decay} (52 ps) in the kinetic fitting of the SESA signal represents the lifetime of singlet exciton decay, implying that the ISC time of compound **5** is approximately 50 ps. For ns-TA spectroscopy, the decay lifetime of T_1–T_n absorption signal is fitted as 4.9 ns.

In Fig. 12, the two spectral components (11 ps and 4.2 ns) in the global fitting of compound **6** are assigned to the exciton decay times of singlet and triplet states, respectively. Moreover, τ_{decay} (12 ps) in the kinetic fitting of SESA signal represents the lifetime of singlet exciton decay. For ns-TA spectroscopy, the decay lifetime of T_1–T_n absorption signal is fitted as 3.9 ns.

APPENDIX B: THEORETICAL SIMULATION RESULTS

As indicated by Table I, for compound **1**, the calculated absorption energy of 323 nm corresponds to experimental absorption peak located at 337 nm, which confirms that the experimental absorption peak is attributable to the $S_0 \rightarrow S_1$ transition. The calculated fluorescence energy for the S_1 state (351 nm) is in agreement with the experimental values (360 nm). These results indicate that under the pump light (337 nm), the molecule **1** is photoexcited to the S_1 state and then emits the fluorescence at 360 nm. The other six molecules undergone the similar process to molecule **1**, which transition directly to the S_1 state.

Table II presents the transition configurations of compound **1** in the singlet and triplet excited states. Compound **1** has the HOMO → LUMO transition configuration (97.7%) in the S_1 state. For the triplet states, the compound **1** has the approximate HOMO → LUMO transition, indicating that the molecule has an effective ISC channel.

Table III presents the transition configurations of compound **2** in the singlet and triplet excited states. Compound **2** has the HOMO → LUMO transition configuration (97.5%) in the S_1 state. For the triplet states, the compound **2** has the approximate HOMO → LUMO transition, indicating that the molecule has an effective ISC channel.

Table IV shows the transition configurations of compound **3** in the singlet and triplet excited states. Compound **3** has the HOMO → LUMO transition configuration (97.4%) in the S_1 state. For the triplet states, compound **3** has the approximate HOMO → LUMO transition, indicating that the molecule has an effective ISC channel.

Table V displays the transition configurations of compound **4** in the singlet and triplet excited states. Compound **4** has the HOMO → LUMO transition configuration (96.9%) in the S_1 state. For the triplet states, compound **4** has the approximate HOMO → LUMO transition, indicating that the molecule has an effective ISC channel.

TABLE I. Calculated absorption and fluorescence energy (nm) of seven molecules.

		1	**2**	**3**	**4**	**5**	**6**	**7**
Abs (nm)	S_1	323	322	319.87	314	332	325	332
	S_2	291	304	303.55	301	291	292	316
	S_3	285	299	295.36	291	288	286	291
Flu (nm)		351	346	346	340	362	356	363

TABLE II. Transition configurations of compound **1** in the singlet and triplet excited states revealed by TDDFT calculations.

	*n*th	Transition configuration
S_n	1	H → L 97.7%
T_n	1	H → L 69.2%, H − 1 → L 23.0%, H → L + 3 2.1%
	2	H − 1 → L 68.4%, H → L 24.8%
	3	H → L + 1 39.8%, H − 3 → L + 1 23.7%, H − 2 → L + 2 11.5%, H-1 → L + 1 11.2%, H − 4 → L + 2 8.1%

TABLE III. Transition configurations of compound **2** in the singlet and triplet excited states revealed by TDDFT calculations.

	*n*th	Transition configuration
S_n	1	H → L 97.5%
T_n	1	H − 1 → L 79.0%, H → L + 4 9.5%, H − 3 → L 4.3%, H − 5 → L + 9 2.6%
	2	H → L 93.1%, H − 3 → L + 4 2.6%
	3	H → L + 1 61.0%, H − 2 → L + 1 21.2%, H − 4 → L + 2 11.4%

TABLE IV. Transition configurations of compound **3** in the singlet and triplet excited states revealed by TD-DFT calculations.

	*n*th	Transition configuration
S_n	1	H → L 97.4%
T_n	1	H → L 73.5%, H − 1 → L 19.6%
	2	H − 1 → L 73.3%, H → L 20.5%
	3	H → L + 1 30.3%, H − 1 → L + 1 20.1%, H − 2 → L + 2 18.5%, H − 4 → L + 1 17.2%, H − 2 → L + 1 3.5%

TABLE V. Transition configurations of compound **4** in the singlet and triplet excited states revealed by TDDFT calculations.

	*n*th	Transition configuration
S_n	1	H → L 96.9%, H − 1 → L + 4 2.2%
T_n	1	H → L 88.6%, H − 1 → L 4.8%, H − 5 → L + 9 2.2%, H − 1 → L + 4 2.2%
	2	H − 1 → L 90.3%, H → L 5.2%
	3	H − 2 → L + 2 42.8%, H − 4 → L + 1 32.5%, H − 2 → L + 1 12.1%, H − 4 → L + 2 5.8%, H − 7 → L + 2 3.3%

TABLE VI. Transition configurations of compound **5** in the singlet and triplet excited states revealed by TDDFT calculations.

	*n*th	Transition configuration
S_n	1	H → L 97.9%
T_n	1	H → L 71.9%, H − 1 → L 19.3%, H → L + 3 2.4%, H − 2 → L 2.0%
	2	H − 1 → L 65.8%, H → L 23.1%, H → L + 3 2.8%
	3	H → L + 1 50.5%, H − 4 → L + 1 10.6%, H − 3 → L + 2 9.6%, H − 3 → L + 1 7.5%, H − 1 → L + 1 4.9%, H-4 → L + 2 4.7%

TABLE VII. Transition configurations of compound **6** in the singlet and triplet excited states revealed by TDDFT calculations.

	*n*th	Transition configuration
S_n	1	H → L 97.7%
T_n	1	H → L 83.9%, H − 1 → L 9.3%
	2	H − 1 → L 84.1%, H → L 9.9%
	3	H − 1 → L + 1 26.1%, H − 3 → L + 1 24.0%, H − 2 → L + 2 20.4%, H → L + 1 18.1%

TABLE VIII. Transition configurations of compound **7** in the singlet and triplet excited states revealed by TDDFT calculations.

	*n*th	Transition configuration
S_n	1	H → L 97.8%
T_n	1	H → L 71.1%, H − 1 → L 19.9%, H − 3 → L 2.3%, H → L + 4 2.3%
	2	H − 1 → L 62.8%, H → L 23.5%, H − 2 → L 3.0%, H → L + 4 2.5%
	3	H − 2 → L + 1 55.8%, H → L + 1 12.7%, H − 5 → L + 2 6.4%, H − 1 → L + 1 6.2%, H − 4 → L + 3 4.8%, H → L + 2 4.5%

Table VI lists the transition configurations of compound **5** in the singlet and triplet excited states. Compound **5** has the HOMO → LUMO transition configuration (97.9%) in the S_1 state. For the triplet states, compound **5** has the approximate HOMO → LUMO transition, indicating that the molecule has an effective ISC channel.

Table VII presents the transition configurations of compound **6** in the singlet and triplet excited states. Compound **6** has the HOMO → LUMO transition configuration (97.7%) in the S_1 state. For the triplet states, compound **6** has the approximate HOMO → LUMO transition, indicating that the molecule has an effective ISC channel.

Table VIII displays the transition configurations of compound **7** in the singlet and triplet excited states. Compound **7** has the HOMO → LUMO transition configuration (97.8%) in the S_1 state. For the triplet states, compound **7** has the approximate HOMO → LUMO transition, indicating that the molecule has an effective ISC channel.

In Table IX, the calculated energies for T_1, T_2, T_3, and T_4 of compound **1** are 3.10, 5.67, 6.18, and 6.72 eV, respectively. In the TA spectroscopy of compound **1**, the triplet-triplet absorption signal located at 410 nm is attributed to the transition from the T_1 state to the T_3 state (3.08 eV, 403 nm), and then decays to the T_1 state by the internal conversion. For the other six molecules, the energy maps between the T_1 and T_3 states are calculated as 3.08 (compound **2**), 3.08 (compound **3**),

TABLE IX. Calculated energies of the higher triplet states.

		1	**2**	**3**	**4**	**5**	**6**	**7**
Energy (eV)	T_1	3.10	3.10	2.90	2.89	2.87	2.82	2.87
	T_2	5.67	5.65	5.43	5.41	5.47	5.27	5.47
	T_3	6.18	6.18	5.98	5.99	5.92	5.86	5.92
	T_4	6.72	6.58	6.41	6.60	6.47	6.48	6.13

TABLE X. Calculated ISC rate for the S_1-T_1 transition of seven molecules.

	1	**2**	**3**	**4**	**5**	**6**	**7**
k_{ISC}	1.9×10^4	2.4×10^4	7.1×10^4	7.0×10^5	2.1×10^6	8.6×10^7	2.9×10^6

3.10 (compound **4**), 3.05 (compound **5**), 3.04 (compound **6**), and 3.05 eV (compound **7**), respectively. These results show that the triplet-triplet absorption signals of all the molecules are attributed to the transition from the T_1 state to the T_3 state.

Table X lists the calculated ISC rate constants for the $S_1 \rightarrow T_1$ transition of the seven molecules. The ISC rate between the S_1 and T_1 states of heavy-atom free compound **1** is calculated to be 1.9×10^4 s^{-1}. When Br atoms are introduced in 9-phenyl unit, the ISC rates are enhanced with the decrease of the spatial distance between bromine atom and carbazole core. Compared with compound **1**, the ISC rate of compounds **2**–**4** changes to 2.4×10^4 s^{-1}, 7.1×10^4 s^{-1}, and 7.0×10^5 s^{-1}, respectively. Furthermore, with bromine substitution on the carbazole core, compounds **5** and **6** have larger ISC rates (2.1×10^6 s^{-1} and 8.6×10^7 s^{-1}, respectively) than those of compounds **2**–**4**. For biphenyl structured compound **7**, the calculated ISC rate (2.9×10^6 s^{-1}) is close to that of compound **5**, which indicates that the biphenyl group has a slight effect on the space heavy-atom effect and ISC process. The calculated ISC rates show that the shortening of spatial distance induces efficient ISC, which is consistent with the results of SOC values.

[1] S. Z. Cai, H. F. Shi, J. W. Li, L. Gu, Y. Ni, Z. C. Cheng, S. Wang, W. W. Xiong, L. Li, Z. F. An, and W. Huang, Visible-light-excited ultralong organic phosphorescence by manipulating intermolecular interactions, Adv. Mater. **29**, 1701244 (2017).

[2] Z. Y. Yang, Z. Mao, X. P. Zhang, D. P. Ou, Y. X. Mu, Y. Zhang, C. Y. Zhao, S. W. Liu, Z. G. Chi, J. R. Xu, Y. C. Wu, P. Y. Lu, A. Lien, and M. R. Bryce, Intermolecular electronic coupling of organic units for efficient persistent room-temperature phosphorescence, Angew. Chem., Int. Ed. **55**, 2181 (2016).

[3] Y. Katsurada, S. Hirata, K. Totani, T. Watanabe, and M. Vacha, Photoreversible ON-OFF recording of persistent room-temperature phosphorescence, Adv. Opt. Mater. **3**, 1726 (2015).

[4] P. Lehner, C. Staudinger, S. M. Borisov, and I. Klimant, Ultra-sensitive optical oxygen sensors for characterization of nearly anoxic systems, Nat. Commun. **5**, 4460 (2014).

[5] X. Zhen, Y. Tao, Z. An, P. Chen, C. Xu, R. Chen, W. Huang, and K. Pu, Ultralong phosphorescence of water-soluble organic nanoparticles for *in vivo* afterglow imaging, Adv. Mater. **29**, 1606665 (2017).

[6] S. M. A. Fateminia, Z. Mao, S. D. Xu, Z. Y. Yang, Z. G. Chi, and B. Liu, Organic nanocrystals with bright red persistent room-temperature phosphorescence for biological applications, Angew. Chem., Int. Ed. **56**, 12160 (2017).

[7] Z. Mao, Z.Yang, Z. Fan, E. Ubba, W. Li, Y. Li, J. Zhao, Z. Yang, M. P. Aldred, and Z. Chi, The methylation effect in prolonging the pure organic room temperature phosphorescence lifetime, Chem. Sci. **10**, 179 (2019).

[8] J. C. Koziar and D. O. Cowan, Photochemical heavy-atom effects, Acc. Chem. Res. **11**, 334 (1978).

[9] M. Mońka, D. Grzywacz, E. Hoffman, V. Ievtukhov, K. Kozakiewicz, R. Rogowski, A. Kubicki, B. Liberek, P. Bojarski, and I. E. Serdiuk, Decisive role of heavy-atom orientation for efficient enhancement of spin–orbit coupling in organic thermally activated delayed fluorescence emitters, J. Mater. Chem. C **10**, 11719 (2022).

[10] F. D. Zhuang, Z. H. Sun, Z. F. Yao, Q. R. Chen, Z. Huang, J. H. Yang, J. Y. Wang, and J. Pei, BN-Embedded tetrabenzopentacene: A pentacene derivative with improved stability, Angew. Chem., Int. Ed. **58**, 10708 (2019).

[11] K. Omoto, T. Nakae, M. Nishio, Y. Yamanoi, H. Kasai, E. Nishibori, T. Mashimo, T. Seki, H. Ito, K. Nakamura, N. Kobayashi, N. Nakayama, H. Goto, and H. Nishihara, Thermosalience in macrocycle-based soft crystals via anisotropic deformation of disilanyl architecture, J. Am. Chem. Soc. **142**, 12651 (2020).

[12] Q. Peng, H. Ma, and Z. Shuai, Theory of long-lived room-temperature phosphorescence in organic aggregates, Acc. Chem. Res. **54**, 940 (2021).

[13] L. Gu, H. Shi, M. Gu, K. Ling, H. Ma, S. Cai, L. Song, C. Ma, H. Li, G. Xing, X. Hang, J. Li, Y. Gao, W.

Yao, Z. Shuai, Z. An, X. Liu, and W. Huang, Dynamic ultralong organic phosphorescence by photoactivation, Angew. Chem., Int. Ed. **57**, 8425 (2018).

[14] C. J. Chen, Z. G. Chi, K. C. Chong, A. S. Batsanov, Z. Yang, Z. Mao, Z. Y. Yang, and B. Liu, Carbazole isomers induce ultralong organic phosphorescence, Nat. Mater. **20**, 175 (2021).

[15] C. Qian, Z. Ma, X. Fu, X. Zhang, Z. Li, H. Jin, M. Chen, H. Jiang, X. Jia, and Z. Ma, More than carbazole derivatives activate room temperature ultralong organic phosphorescence of benzoindole derivatives, Adv. Mater. **34**, 2200544 (2022).

[16] Y. Gong, G. Chen, Q. Peng, W. Z. Yuan, Y. Xie, S. Li, Y. Zhang, and B. Z. Tang, Achieving persistent room temperature phosphorescence and remarkable mechanochromism from pure organic luminogens, Adv. Mater. **27**, 6195 (2015).

[17] B. Li, Y. Gong, L. Wang, H. Lin, Q. Li, F. Guo, Z. Li, Q. Peng, Z. Shuai, L. Zhao, and Y. Zhang, Highly efficient organic room-temperature phosphorescent luminophores through tuning triplet states and spin-orbit coupling with incorporation of a secondary group, J. Phys. Chem. Lett. **10**, 7141 (2019).

[18] J. A. Joule, Recent advances in the chemistry of 9*H*-carbazoles, Adv. Heterocycl. Chem. **35**, 83 (1984).

[19] C. W. Lee, J.-K. Kim, S. H. Joo, and J. Y. Lee, High quantum efficiency blue phosphorescent organic light-emitting diodes using 6-position-modified benzofuro[2,3-*b*]pyridine derivatives, ACS Appl. Mater. Interfaces **5**, 2169 (2013).

[20] K. Gao, K. Liu, X.-L. Li, X. Cai, D. Chen, Z. Xu, Z. He, B. Li, Z. Qiao, D. Chen, Y. Cao, and S.-J. Su, An ideal universal host for highly efficient full-color, white phosphorescent and TADF OLEDs with a simple and unified structure, J. Mater. Chem. C **5**, 10406 (2017).

[21] Z. Li, Z. Cheng, J. Lin, N. Xie, C. Li, G. Yang, and Y. Wang, Isomer dependent molecular packing and carrier mobility of *N*-phenylcarbazole-phenanthro[9,10-*d*]imidazole based materials as hosts for efficient electrophosphorescence devices, J. Mater. Chem. C **7**, 13486 (2019).

[22] G. L. Thornton, R. Phelps, and A. J. Orr-Ewing, Transient absorption spectroscopy of the electron transfer step in the photochemically activated polymerizations of *N*-ethylcarbazole and 9-phenylcarbazole, Phys. Chem. Chem. Phys. **23**, 18378 (2021).

[23] S. Lower and M. El-Sayed, The triplet state and molecular electronic processes in organic molecules, Chem. Rev. **66**, 199 (1966).

[24] M. A. El-Sayed, Triplet state. Its radiative and nonradiative properties, Acc. Chem. Res. **1**, 8 (1968).

[25] Y. Nagai, H. Sasabe, S. Ohisa, and J. Kido, Effect of substituents in a series of carbazole-based host-materials toward high-efficiency carbene-based blue OLEDs, J. Mater. Chem. C **4**, 9476 (2016).

[26] H. Shi, L. Song, H. Ma, C. Sun, K. Huang, A. Lv, W. Ye, H. Wang, S. Cai, W. Yao, Y. Zhang, R. Zheng, Z. An, and W. Huang, Highly efficient ultralong organic phosphorescence through intramolecular-space heavy-atom effect, J. Phys. Chem. Lett. **10**, 595 (2019).

[27] H. Sasabe, J.-i. Takamatsu, T. Motoyama, S. Watanabe, G. Wagenblast, N. Langer, O. Molt, E. Fuchs, C. Lennartz, and J. Kido, High-efficiency blue and white organic light-emitting devices incorporating a blue iridium carbene complex, Adv. Mater. **22**, 5003 (2010).

[28] S. La Paglia, The electronic spectra of the group IV tetraphenyls, J. Mol. Spectrosc. **7**, 427 (1961).

[29] J. B. Birks, *Photo Physics of Aromatic Molecules* (Wiley-Interscience, 1970). p. 264.

[30] J. Z. Zhao, K. J. Xu, W. B. Yang, Z. J. Wang, and F. F. Zhong, The triplet excited state of Bodipy: Formation, modulation and application, Chem. Soc. Rev. **44**, 8904 (2015).

[31] S. H. Lim, C. Thivierge, P. Nowak-Sliwinska, J. Han, H. van den Bergh, G. Wagnieres, K. Burgess, and H. B. Lee, *In vitro* and *in vivo* photocytotoxicity of boron dipyrromethene derivatives for photodynamic therapy, J. Med. Chem. **53**, 2865 (2010).

[32] W. Wu, H. Guo, W. Wu, S. Ji, and J. Zhao, Organic triplet sensitizer library derived from a single chromophore (BODIPY) with long-lived triplet excited state for triplet-triplet annihilation based upconversion, J. Org. Chem. **76**, 7056 (2011).

[33] Y. Yang, Z. Jiang, Y. Liu, T. Guan, Q. Zhang, K. Jiang, C. Qin, and Y. F. Liu, Transient absorption spectroscopy of a carbazole-based room-temperature phosphorescent molecule: Real-time monitoring of singlet-triplet transitions, J. Phys. Chem. Lett. **13**, 9381 (2022).

[34] Y. Yang, Y. Liu, B. Feng, H. Zhang, C. Qin, K. Yu, K. Jiang, and Y. F. Liu, Discerning the multi-color fluorescence in donor-*n*-acceptor molecules by femtosecond transient absorption spectroscopy, J. Lumin. **242**, 118591 (2022).

[35] W. Kohn and L. J. Sham, Self-consistent equations including exchange and correlation effects, Phys. Rev. **140**, A1133 (1965).

[36] R. G. Parr, in *Horizons of Quantum Chemistry*, edited by K. Fukui and B. Pullman (Springer, Dordrecht, 1980), pp. 5–15.

[37] R. Car and M. Parrinello, Unified approach for molecular dynamics and density-functional theory, Phys. Rev. Lett. **55**, 2471 (1985).

[38] A. D. Becke, Density-functional thermochemistry. IV. A new dynamical correlation functional and implications for exact-exchange mixing, J. Chem. Phys. **104**, 1040 (1996).

[39] C. Lee, W. Yang, and R. G. Parr, Development of the Colle-Salvetti correlation-energy formula into a functional of the electron density, Phys. Rev. B **37**, 785 (1988).

[40] K. Eichkorn, F. Weigend, O. Treutler, and R. Ahlrichs, Auxiliary basis sets for main row atoms and transition metals and their use to approximate Coulomb potentials, Theor. Chem. Acc. **97**, 119 (1997).

[41] F. Weigend and R. Ahlrichs, Balanced basis sets of split valence, triple zeta valence and quadruple zeta valence quality for H to Rn: Design and assessment of accuracy, Phys. Chem. Chem. Phys. **7**, 3297 (2005).

[42] M. J. Frisch, *et al.*, GAUSSIAN *16, Revision C.01* (Gaussian, Inc., Wallingford CT, 2016).

[43] A. V. Marenich, C. J. Cramer, and D. G. Truhlar, Universal solvation model based on solute electron density and on a continuum model of the solvent defined by the bulk dielectric constant and atomic surface tensions, J. Phys. Chem. B **113**, 6378 (2009).

[44] F. Neese, The ORCA program system, Wiles, Comput. Mol. Sci. **2**, 73 (2012).

[45] Q. Peng, Y. Yi, Z. Shuai, and J. Shao, Toward quantitative prediction of molecular fluorescence quantum efficiency: Role of Duschinsky rotation, J. Am. Chem. Soc. **129**, 9333 (2007).

[46] Y. Niu, Q. Peng, and Z. Shuai, Promoting-mode free formalism for excited state radiationless decay process with Duschinsky rotation effect, Sci. China, Ser. B: Chem. **51**, 1153 (2008).

[47] P. Li, Y. Guo, Y. Jia, H. Guan, C. Wang, Z. Wu, S. Sun, Z. Qu, P. Zhou, and G. Zhao, Achieving metal-free phosphorescence in dilute solutions for imaging hypoxia in cells and tumors, Mater. Chem. Front. **5**, 7170 (2021).

[48] S. Li, X. Jin, Z. Yu, X. Xiao, H. Geng, Q. Liao, Y. Liao, Y. Wu, W. Hu, and H. Fu, Design of thermally activated delayed fluorescent emitters for organic solid-state microlasers, J. Mater. Chem. C **9**, 7400 (2021).

[49] H. Zhang, L. Ke, Z. Li, Y. Nie, J. Wang, H. Bi, and Y. Wang, Vibronic transitions determined narrowband emission for multi-resonant thermally activated delayed fluorescence emitters, J. Mater. Chem. C **11**, 9300 (2023).

[50] J. Liu, H. Su, L. Meng, Y. Zhao, C. Deng, J. C. Y. Ng, P. Lu, M. Faisal, J. W. Y. Lam, X. Huang, H. Wu, K. S. Wong, and B. Z. Tang, What makes efficient circularly polarised luminescence in the condensed phase: Aggregation-induced circular dichroism and light emission, Chem. Sci. **3**, 2737 (2012).